Room-temperature mid-infrared laser sensor for trace gas detection

Thomas Töpfer, Konstantin P. Petrov, Yasuharu Mine, Dieter Jundt, Robert F. Curl, and Frank K. Tittel

Design and operation of a compact, portable, room-temperature mid-infrared gas sensor is reported. The sensor is based on continuous-wave difference-frequency generation (DFG) in bulk periodically poled lithium niobate at 4.6 μm, pumped by a solitary GaAlAs diode laser at 865 nm and a diode-pumped monolithic ring Nd:YAG laser at 1064.5 nm. The instrument was used for detection of CO in air at atmospheric pressure with 1 ppb precision (parts in 10^9, by mole fraction) and 0.6% accuracy for a signal averaging time of 10 s. It employed a compact multipass absorption cell with a 18-m path length and a thermoelectrically cooled HgCdTe detector. Precision was limited by residual interference fringes arising from scattering in the multipass cell. This is the first demonstration of a portable high-precision gas sensor based on diode-pumped DFG at room temperature. The use of an external-cavity diode laser can provide a tuning range of 700 cm^{-1} and allow the detection of several trace gases, including N_2O, CO_2, SO_2, H_2CO, and CH_4.

Key words: Trace gas detection, mid-infrared spectroscopy, difference-frequency generation, diode-pumped difference-frequency generation, quasi-phase-matching, periodically poled lithium niobate, gas sensors.

1. Introduction

In recent years there has been an increasing interest in detection and precise measurement of environmentally important atmospheric trace gases such as nitric oxide (NO), carbon monoxide (CO), nitrous oxide (N_2O), formaldehyde (H_2CO), methane (CH_4), and sulfur dioxide (SO_2). Applications that require such measurements include air quality control, atmospheric chemistry, mapping of agricultural, landfill, and traffic emission, and pipeline leak detection. Applications such as landfill emissions monitoring require measurements of gas fluxes and isotopic ratios in addition to gas concentration.

Mid-infrared spectroscopy based on laser difference-frequency generation (DFG)[1–9] is a convenient technique for trace gas detection in that it combines high-speed, high-precision, remote sensing capabilities and convenient access to wavelengths suitable for sensitive detection. Recent advances in diode lasers and novel infrared nonlinear materials permit the development of compact, portable laser-based field instruments for trace gas detection in open air. Such instruments can provide cost-effective solutions to problems of air quality monitoring, offering adequate sampling speed, high-precision, long-lifetime, low-maintenance operation at room temperature and low power consumption.

There are several competing technologies in mid-infrared atmospheric sensing. Fourier transform infrared and lead-salt diode lasers systems, which are semiportable, are currently used in the field. (We define a portable sensor as one in which one strong person can carry the sensor sans power source over long distances; a semiportable sensor can be moved from location to location by truck and set up reasonably conveniently in the new location.) As compared with readily portable Fourier transform infrared sensors, which typically have a resolution of 1 cm^{-1} or greater, DFG offers real individual pressure-broadened or even Doppler-broadened line resolution. Room-temperature operation provides a significant advantage to diode-pumped DFG as compared with lead-salt diode lasers,[10–12] which require cryogenic cooling for normal operation. A promising development, but one unrealized for sensing applications, of electrically and optically pumped type III–V

T. Töpfer, K. P. Petrov, Y. Mine, R. F. Curl, and F. K. Tittel are with the Rice Quantum Institute, Rice University, 6100 Main, Houston, Texas 77005. D. Jundt is with Crystal Technology, Inc., 1040 East Meadow Circle, Palo Alto, California 94303.

Received 24 January 1997; revised manuscript received 30 April 1997.

0003-6935/97/308042-08$10.00/0

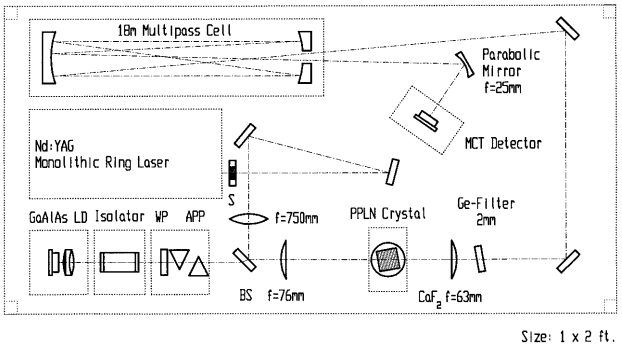

Fig. 1. Diagram of the optical section of a portable sensor for trace gas detection, based on diode-pumped mid-infrared DFG in bulk PPLN. The size of the section is 65 cm × 31 cm × 15 cm. Here WP is a half-wave plate, APP is an anamorphic prism pair, S is a shutter, and BS is a beam splitter.

semiconductor lasers at 2.0–4.5 μm has been reported.[13,14] To date these lasers still require cooling to ~100 K for continuous-wave (cw) operation, but eventually operation at temperatures above 200 K is expected, at which time they may become useful for infrared monitoring. Operation of cw quasi-phase-matched optical parametric oscillators has also been reported.[15–17] Diode-pumped cw optical parametric oscillators may become attractive sources for use in high-resolution spectroscopy and trace gas detection, but further development is needed to alleviate their present shortcomings. These include unreliable single-frequency operation and lack of predictable fast wavelength control.

The purpose of this work was to construct a portable all-solid-state gas sensor based on diode-pumped mid-infrared DFG and to achieve detection limits of better than 10 parts in 10^9 (ppb) for some important trace gases in air at atmospheric pressure. Earlier feasibility tests[18–20] have indicated that this can be done with the use of periodically poled lithium niobate (PPLN), a novel infrared nonlinear material that is now commercially available. Its quasi-phase-matching properties can be tailored for DFG in the 2–5-μm region with many commercial diode and diode-pumped solid-state lasers. This, along with large nonlinearity and good optical quality, makes PPLN the ideal mixing material for DFG applications targeted at species such as CO, N_2O, CO_2, SO_2, H_2CO, and CH_4 (Refs. 21, 22). Here we report design, construction, and performance testing of an all-solid-state DFG sensor for carbon monoxide. The sensor is portable but is not yet rugged enough for portable field operations. It has been operated in the field as a semiportable device.

2. Instrument Description

A diagram of the optical section of the gas sensor is shown in Fig. 1. Our choice of the laser pump sources was motivated primarily by their capability of reliable single-frequency, low-noise operation over extended periods of time in an environment where vibration and changes in temperature and humidity are commonplace. The signal source is a diode-pumped nonplanar monolithic ring Nd:YAG laser with 750-mW output power at 1064.5 nm (Lightwave Electronics, Inc., Model 126). The pump source is a 100-mW solitary GaAlAs diode laser at 865 nm (SDL, Inc., Model 5412), hermetically sealed in a TO-3 metal package together with a thermoelectric cooler, a monitor photodiode, and a thermistor. The laser is attached to a stable mirror mount, and its output is collimated by an f = 8-mm multielement lens with 8-mm aperture. The lens is held by two eccentric rings mounted in the adjustable front plate of the mirror mount. Such an arrangement provided precise, long-term stable alignment of the lens in three dimensions with minimum sensitivity to vibration.

The output of the diode laser passes through a compact 40-dB isolator with an 8 mm × 2 mm rectangular aperture (Electro-Optics Technology, Inc., Model 1845), a half-wave plate, and a 4× anamorphic prism pair, emerging as a vertically polarized beam 1.9 mm in diameter and nearly mode matched to the signal beam for efficient DFG. The pump and signal beams are combined by a dichroic beam splitter and focused by an f = 75-mm lens into an uncoated PPLN crystal measuring 19 mm × 11 mm × 0.5 mm (Crystal Technology, Inc.). The z-cut crystal has eight 1.3-mm-wide strips with domain-grating periods ranging from 22.4 to 23.1 μm in 0.1-μm steps. For difference-frequency mixing at 4.6 μm (idler), the optimum period was found to be 22.9 μm at room temperature. Data from Edwards *et al.*[16] suggest a domain-grating period of 23.3 μm for quasi-phase-matching at this wavelength. This discrepancy is due to the uncertainty in the refractive index of lithium niobate at wavelengths longer than 3.5 μm.

The pump and signal beams enter the PPLN crystal at near normal incidence to the domain grating. With P_1 = 70 mW of pump power at 865 nm and P_2 = 750 mW of signal power at 1064.5 nm incident on the crystal, a typical idler power of P_3 = 4.4 μW was measured. This compares reasonably well with 5.5 μW calculated from the theory of Chu and Broyer[23] with the effective nonlinear coefficient of $d_{\text{eff}} = (2/\pi)$ 27 pm V^{-1}:

$$P_3 = \frac{(16\pi\omega_3 d_{\text{eff}})^2}{c^2 n_1 n_2 n_3 (k_1^{-1} + k_2^{-1})} P_1 P_2 L h\left(\frac{L}{b}; \frac{k_2}{k_1}\right) T \exp(-\alpha L),$$

where

$$h(\xi; \mu) = \frac{1}{2\xi} \int_0^{\xi} d\tau'' \int_{-\xi}^{\xi} \times d\tau' \frac{1 + \tau'\tau''}{(1 + \tau'\tau'')^2 + (\tau' - \tau'')^2 \cdot \left(\frac{\mu^2 - 1}{\mu^2 + 1}\right)^2}.$$

Here k_i are wave vectors, n_i are indices of refraction, L = 19 mm is the crystal length, b = 8 mm is the confocal parameter of the mode-matched pump and signal beams, and $1 - T$ = 34% is the combined loss

from Fresnel reflection at the input and the output faces of the crystal. The factor $\exp(-\alpha L)$ accounts for significant linear absorption losses in $LiNbO_3$ at 4.6 μm. Measurements by Myers[24] suggest transmission of only 38% for the extraordinary beam in a 19-mm-long PPLN crystal at this wavelength. A ~25% discrepancy between measured and calculated power is due in part to clipping of the rapidly diverging idler beam at the output face of the crystal. DFG conversion efficiency was also reduced because of nonoptimal overlap between pump and signal beams, which both had elliptical shape.

The idler beam is collimated with an $f = 63$ mm uncoated calcium fluoride lens and separated from the pump and signal beams by a germanium filter. The idler beam is then directed into a compact multipass cell (New Focus, Inc., Model 5611) aligned for an effective path length of 18.3 m. The cell was used to increase the measured optical absorption by CO in air to at least 1%, so that the measured signal may substantially exceed detector noise and optical interference. Absorption signals of this magnitude could be easily observed in the presence of linear amplitude modulation associated with frequency tuning of the pump laser. The path length of 18.3 m is achieved with 92 passes between mirrors separated by 20 cm. Optical throughput of the cell was measured to be 38%. An $f = 35$ mm off-axis parabolic mirror collected the idler beam at the output of the cell.

Measurements of idler power were initially performed with the use of a liquid-nitrogen-cooled photovoltaic InSb detector. The results were used to calibrate the response of a HgCdTe detector with 1-mm^2 active area (EG&G Judson, Inc., Model J15TE3:5), cooled to −65 °C by a three-stage Peltier cooler. The detector is biased at 1.2 mA and dc coupled to a low-noise preamplifier with a voltage gain of 350 and a gain bandwidth of 200 kHz. The detector/preamplifier system has a response of 0.46 V μW^{-1} and a noise-equivalent power of 3.3 pW $Hz^{-1/2}$ at 4.6 μm, with a typical output voltage drift of 0.25 mV h^{-1} in the dark state. Low-drift dc coupling of the detector allowed the direct measurement of idler power necessary to determine percent optical absorption. Typical idler power measured after the multipass cell was 1.5 μW.

Output of the preamplifier was digitized with a 12-bit, 100-kS/s analog-to-digital converter, part of a compact data acquisition card (National Instruments, Inc., DAQCard-1200). The card served as an interface to a laptop computer (Fig. 2). Digital output of the card was used to control a small mechanical shutter to block the Nd:YAG beam for 10 s every 3 min, allowing the measurement of dark detector voltage.

The spectroscopic information collected consisted of the detector voltage, $V(x)$, as a function of the wavelength sweep signal to the diode current controller, x, and the dark voltage V_{dark}. A time trace of detector voltage $V(x)$ averaged over 10–1000 sweeps, with dark voltage V_{dark} subtracted, constituted a spectroscopic measurement. Depending on the number of averages, the result could be updated every 1–20 s. For short scans, the diode frequency and thus the idler frequency can be considered to be a linear function of x, $\nu = A + Bx$. The frequency sweep is a linear function of time because tuning is performed by a triangular waveform. Thus, acquiring the detector voltage as function of time is equivalent to acquiring it as function of x or ν. At any point in the scan, the Beer–Lambert law for the power transmitted in the presence of CO, $P(\nu)$, as compared with the power transmitted in the absence of CO, $P_0(\nu)$, is

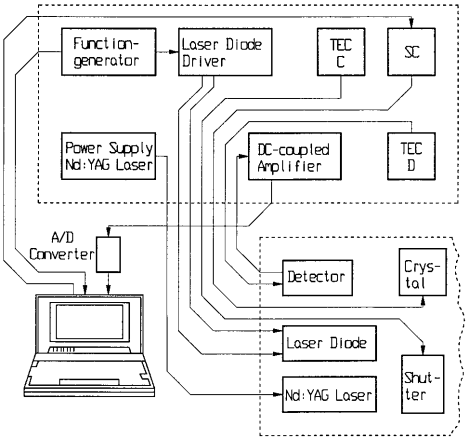

Fig. 2. Diagram of the electronic section of the instrument. A logic signal from the laptop computer drives the shutter circuit (SC) to periodically block the Nd:YAG beam for measurements of dark detector voltage.

$$P(\nu) = P_0(\nu)\exp[-\gamma(\nu)CL],$$

where $\gamma(\nu)$ is the absorptivity, C is the concentration of CO, and L is the path length of the cell. The actual dependence on ν of $\gamma(\nu)$ is expected to be the Voigt function, but at 1 atm of pressure the ν dependence of $\gamma(\nu)$ is well approximated by the much simpler Lorentzian profile,

$$\gamma(\nu) = \frac{\gamma_0}{1 + [(\nu - \nu_0)/\Delta]^2}.$$

Thus, if we assume that $(V - V_{\text{dark}})$ is proportional to the infrared power P and that P_0 is a linear function of x, we can substitute into the Beer–Lambert equation to obtain

$$\ln[V(x) - V_{\text{dark}}] = \frac{a_0}{1 + (x - a_1)^2/{a_2}^2} + \ln(a_3 + a_4 x).$$

Here $a_0 = C\gamma_0 L$ is the peak absorbance, a_1 is the peak center (corresponding to ν_0), a_2 is the peak half-width at half-maximum (corresponding to Δ), and $a_3 + a_4 x$ accounts for the linear modulation of the idler power P_0 associated with the frequency sweep. The above equation was employed in nonlinear least-squares fitting of absorption spectra with use of the Levenberg–Marquardt method.[25] Typical values of peak absorbance a_0 observed for the $R(2)$ transition of

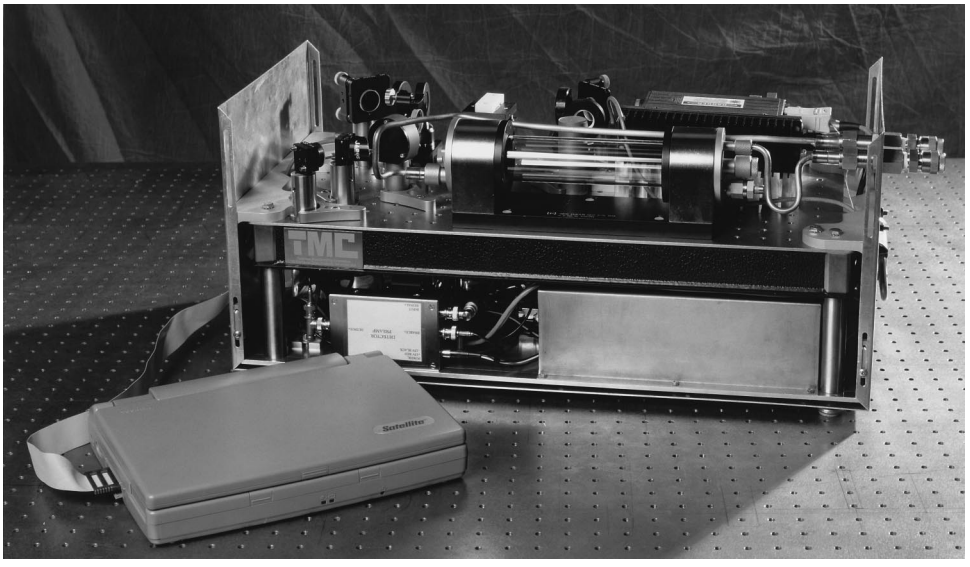

Fig. 3. Photograph of the instrument with cover removed, showing the optical breadboard and the electronic components mounted below.

CO in room-temperature air were 0.01–0.02; they were used to compute the CO mole fraction in parts in 10^9 based upon the calibration determining $C\gamma_0 L$ described below.

Direct absorption spectroscopy was chosen in this application because it offers adequate precision combined with the ease of signal processing and calibration. Alternatively, wavelength-modulation spectroscopy[26] can be used, provided the modulation frequency falls within the gain bandwidth of the detector–preamplifier. This method is attractive because of an efficient reduction of noise bandwidth. However, it requires more sophisticated signal processing and calibration techniques.

The entire optical setup along with power supplies and electronics is contained in a 31 cm × 31 cm × 65 cm aluminum case (Fig. 3). The instrument draws less than 50 W of electrical power and can be operated from car batteries.

3. Spectroscopic Measurements

Idler frequency scans were performed by a 58-Hz, 30-mA peak-to-peak triangular modulation of the diode laser drive current. This corresponds to a tuning range of approximately 30 GHz, sufficient for capturing a single atmospheric pressure-broadened transition of CO.

Nitrous oxide (N_2O) was used as a reference gas to determine the operating wavelength. The setting reproducibility of the diode laser temperature controller and current were sufficiently accurate to relocate the CO line frequency in the subsequent measurements. Of course, the line center a_1 was redetermined by the fitting described above for each set of averaged traces. Figure 4 shows a portion of the reference spectrum near 2154.5 cm^{-1} at a pressure of 2.5 Pa in the multipass cell, with a correction made for the linear amplitude modulation associated with frequency tuning. The trace is a 512 sweep average. The observed transitions were identified with the help of Refs. 22 and 27 and are listed in Table 1. Peaks 7 and 9 could not be identified with the available literature. Their frequencies are given with an uncertainty equal to the maximum deviation of the experimental frequency axis from a straight line, based on the assignments in Ref. 22. Peak 5 was identified as the $R(2)$ fundamental transition of CO. Frequency resolution of the instrument was better than 200 MHz, inferred from the spectroscopy of the $P(28)$ doublet of N_2O near 2169.2 cm^{-1}. We observed interference fringes in the multipass cell caused by scattering, as indicated by the ×200 magnified section of Fig. 4. This interference limited the signal-to-noise ratio to 300 in the averaged trace. The trace contains 1024 points, which can be transformed to yield 513 Fourier components. The signal-to-noise ratio can be improved to better than 10,000 by application of a low-pass Gaussian filter F_k that weighs the higher-frequency Fourier components of the trace to zero:

$$F_k = \exp[-k^2/32^2], \qquad k = 0, \ldots, 512.$$

Figure 5 shows a spectrum of the $R(2)$ fundamental transition [2154.595582 cm^{-1} (Ref. 22)] of CO in dry room-temperature air at atmospheric pressure. Air temperature and humidity were not monitored in this experiment. The dots represent the measured data, a 100 sweep average corrected for the linear amplitude modulation associated with frequency tuning. The thick solid trace is a fit to a Lorentzian profile. The CO mole fraction computed from the fit is 324 ± 6 ppb. The error given corresponds to the root mean squared (rms) fit residuals, plotted with a thin solid curve. The relatively high frequency interference fringes result from scattering in the multipass cell. An absorption line of water at 2154.7 cm^{-1} produces noticeably large fit residuals to the

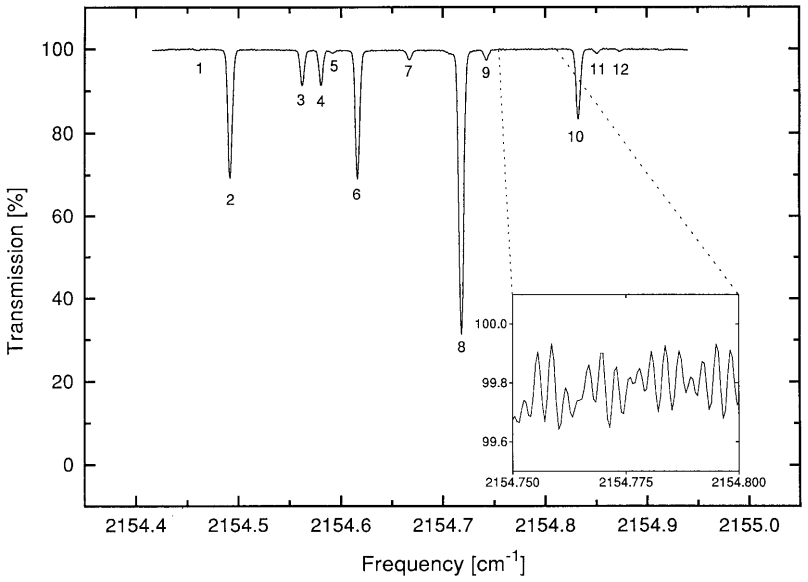

Fig. 4. Infrared spectrum of N_2O in the multipass cell at a pressure of 2.5 Pa. Table 1 lists the corresponding transition frequencies. The trace is a 512 sweep average, corrected for the amplitude modulation associated with frequency tuning. The inset shows magnified interference fringes due to scattering in the multipass cell, limiting the signal-to-noise ratio to 300.

right of the CO absorption peak, even though the measurement was performed in a dry, air-conditioned laboratory. Combined peak-to-peak interference from water vapor and optical fringes in this trace is equivalent to a maximum of 20 ppb CO. The error will increase if the measurements are performed in humid air. Several other transitions of CO, including $R(6)$, are better suited for sensitive detection. We estimate, based on the HITRAN data,[21] that the spectroscopic interference from water under standard conditions (partial pressure of 7.7×10^{-3} atm) can be reduced an equivalent of ~10 ppb CO if detection is performed at the $R(6)$ transition at 2169.19795 cm^{-1} (Ref. 22). We were unable to obtain long-term stable operation of the DFG source at this frequency because of longitudinal mode hops in the diode pump laser.

For calibration of the DFG sensor we measured absorption by CO in air flowing from a high-pressure cylinder (Scott Specialty Gases, Inc.). The factory-assigned CO mole fraction in the cylinder was 9000 ± 50 ppb. The measurements were performed at a flow rate of 300 cm^3 min^{-1} at atmospheric pressure, with 2.5-s interval between data points for 100 s (Fig. 6), and yielded the absorbance $a_0 = 0.5382 \pm 0.0005$. The quantity 0.0005 is the standard deviation of individual values of absorbance. The typical value of the rms fit residuals in this experiment was 0.0013 absorption units, equivalent to 20 ppb CO. The primary sources of the fitting error were interference by water and the fact that the fitting was performed to a Lorentzian rather than a Voigt profile. The value of absorbance, a_0, normalized to CO mole fraction in the sample is the calibration constant:

$$c = \gamma_0 L = (5.980 \pm 0.006) \times 10^{-5}\ \text{ppb}^{-1}.$$

The error given here does not include the uncertainty in concentration of the reference sample. Including this uncertainty implies a calibration constant of $c =$

Table 1. Infrared Transitions Identified in Fig. 4

Transition	Frequency (cm^{-1})	Isotopomer	Rotational Assignment	Vibrational Assignment	Reference
1	2154.46138	$^{15}N^{14}N^{16}O$	$P(22)$	$10^10–10^00$	27
2	2154.49222	$^{14}N^{14}N^{16}O$	$P(54)$	$11^10–10^{1f}0$	22
3	2154.5644	$^{14}N^{15}N^{16}O$	$P(11)$	$11^10–01^{1f}0$	22
4	2154.5839	$^{14}N^{15}N^{16}O$	$P(11)$	$11^10–01^{1e}0$	22
5	2154.595583	$^{12}C^{16}O$	$R(2)$	1–0	22
6	2154.62121	$^{14}N^{14}N^{16}O$	$P(54)$	$11^10–01^{1e}0$	22
7	2154.665 ± 0.005	not identified	not identified	not identified	not identified
8	2154.72236	$^{14}N^{15}N^{16}O$	$P(25)$	$10^00–00^00$	22
9	2154.740 ± 0.005	not identified	not identified	not identified	not identified
10	2154.8324	$^{14}N^{14}N^{16}O$	$P(42)$	$12^00–02^00$	22
11	2154.85091	$^{15}N^{14}N^{16}O$	$P(21)$	$02^12–02^02$	27
12	2154.87288	$^{14}N^{15}N^{16}O$	$R(4)$	$02^12–02^{0f,e}2$	27

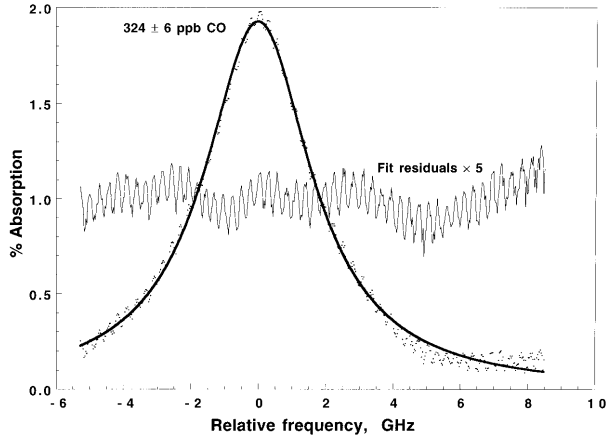

Fig. 5. Spectrum of the $R(2) = 2154.595582\ \mathrm{cm}^{-1}$ (Ref. 22) fundamental transition of CO in room air at atmospheric pressure. The dots represent absorption signal averaged over 100 sweeps and corrected for the linear amplitude modulation associated with frequency tuning. The thick solid trace is a fit to a Lorentzian peak. Frequency axis is drawn relative to the fitted peak center a_1. The frequency scale is based on the pressure-broadening coefficient of $0.068\ \mathrm{cm}^{-1}\ \mathrm{atm}^{-1}$ (Ref. 21) and the fitted peak width a_2.

$(5.98 \pm 0.04) \times 10^{-5}\ \mathrm{ppb}^{-1}$. This compares well with the number $(5.95 \pm 0.06) \times 10^{-5}\ \mathrm{ppb}^{-1}$ calculated from the HITRAN database,[21] assuming an optical path length of 18.3 ± 0.2 m.

Similar measurements were performed over 3 weeks with a cylinder of calibrated dry air with factory-assigned CO mole fraction of 1030 ± 55 ppb. Here we used the previously determined calibration constant c to compute the CO mole fraction from absorbance a_0 (Fig. 7). The measurements yielded typical standard deviations of 1–3 ppb for the signal averaging time of 20 s. The accuracy of these measurements was 0.6%, limited by uncertainty in assignment of the reference sample (9000 ± 50 ppb).

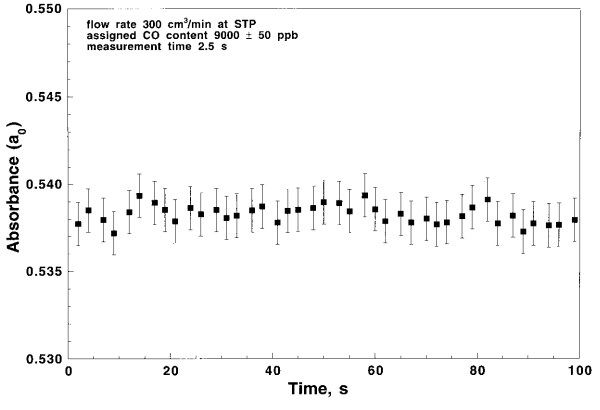

Fig. 6. Peak absorbance (a_0) at the $R(2)$ transition of CO versus time in the calibration experiment. The air from a high-pressure cylinder has a factory-assigned CO content of 9000 ± 50 ppb. The measured absorbance normalized to the CO concentration is $(5.980 \pm 0.006) \times 10^{-5}\ \mathrm{ppb}^{-1}$. This compares well with the number $(5.95 \pm 0.06) \times 10^{-5}\ \mathrm{ppb}^{-1}$ calculated from the HITRAN database.[21] Error bars in the plot represent the root-mean-squared fit residuals, equivalent to 20 ppb CO.

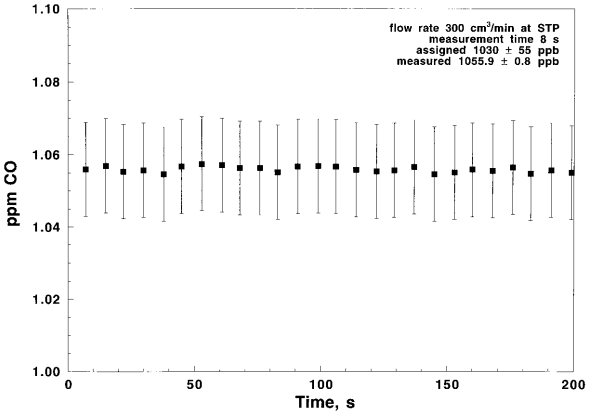

Fig. 7. Measurement of air sample with factory-assigned CO content of 1030 ± 55 ppb. The value measured in the experiment is 1055.9 ± 0.8 ppb, based on the calibration data from Figure 6. Error bars represent the root-mean-squared fit residuals, equivalent to 13 ppb CO.

Unattended operation of the instrument was recorded over extended periods of time to allow us to investigate the drift in alignment, output power, frequency, and spectroscopic baseline profile. Maximum frequency drift observed in a course of a day was ~0.4 GHz. The drift was tracked (in the form of a_1) by the data fitting algorithm and did not affect the measurements of concentration. Infrared output power showed a typical 20% peak-to-peak variation in a course of a day. The variation appears to be caused in part by thermal drift in optical alignment, because at the end of each 24-hour period the level of output power could be recovered by realignment. We did not investigate the effect of photorefractive beam distortion on the efficiency of DFG, even though the PPLN crystal produced a visible amount of light at the second harmonic of the Nd:YAG laser. Optical alignment of the instrument was optimized repeatedly during 3 months of laboratory tests, leading to an overall increase in output power. We were therefore unable to detect any long-term effect of photorefractive damage to the PPLN crystal. Analysis of the photorefractive effect in PPLN[28] and its influence on DFG is beyond the scope of this paper.

Figure 8 shows a record of CO concentration in conditioned laboratory air over 24 hours. The multipass cell was left open in this experiment to allow a convective flow of air. Each data point corresponds to a 512 sweep average acquired every 10 s. The two peaks in Fig. 7 were observed during the morning and evening rush hours and appear somewhat delayed in time. We have recorded such behavior of the CO concentration on a consistent basis over 6 weeks. The stability of the spectroscopic baseline profile was judged by the value of the rms fit residuals, which did not vary by more than 50%, despite the sometimes large swings in the magnitude of absorption signal (Fig. 8).

The instrument can be modified for the detection of other trace gases. The simplest method is to tune the pump wavelength by temperature control to

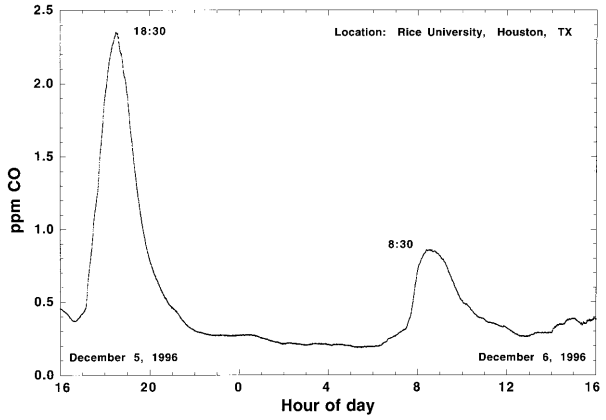

Fig. 8. CO concentration in room air versus time, recorded at Rice University on 5–6 December 1996. The multipass cell was left open to allow convective flow of air. The peaks were observed during the evening and morning rush hours.

reach the desired idler wavelength. A tuning range of ~50 cm^{-1} can be achieved this way. Alternatively, an external-cavity diode laser (SDL, Inc., Model 8610, for example) can provide a tuning range of ≥700 cm^{-1} (816–865 nm). Adjustment of the PPLN grating period will be required in either case and can be performed with the use of a single crystal such as the one described above. Figure 9 shows various molecular species that we believe can be detected with the use of DFG in PPLN, pumped by a tunable near-infrared diode laser, and a Nd:YAG laser at 1064.5 nm. Thicker lines indicate stronger absorption.[21] Table 2 lists the wavelengths necessary to detect each species,[21] the required PPLN domain-grating period,[16] and an estimate of concentration that can be detected with 1% accuracy. All listed transitions were selected to be free from interference by other atmospheric trace gases, including water vapor.

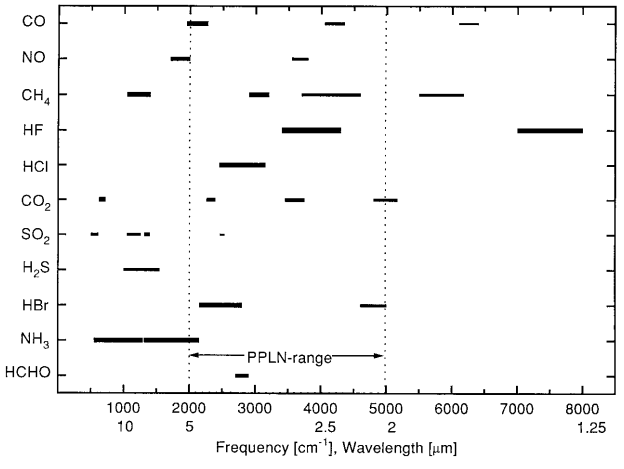

Fig. 9. The range of mid-infrared transitions for various atmospheric pollutants is shown. Data were taken from the HITRAN database.[21]

4. Summary

We described a portable solid-state mid-infrared spectrometer capable of fast measurements of carbon monoxide (CO) in air at atmospheric pressure. The instrument is based on quasi-phase-matched DFG in PPLN at room temperature, pumped by a 100-mW solitary diode laser at 865 nm and a 750-mW diode-pumped monolithic ring Nd:YAG laser at 1064.5 nm. The instrument produced 4.4-μW output power at 4.6 μm with less than 200-MHz linewidth. Spectroscopic detection of CO was performed in air at atmospheric pressure and room temperature, flowing through a compact multipass cell with 18.3-m path length. For CO concentrations between 100 and 9000 ppb, precision of 1 ppb was obtained for a signal averaging time of 20 s. Precision was limited by interference fringes from scattering in the multipass cell. The accuracy of the measurements was limited by the initial accuracy of the air sample used for calibration (0.6%).

This is the first demonstration of a portable, high-precision gas sensor based on diode-pumped mid-infrared DFG. The instrument employs no cryogenic or high-voltage components, measures 31 cm × 31 cm × 65 cm, and is controlled by a laptop computer. It showed reliable unattended operation for more than 36 hours, without appreciable loss of output power or precision.

This technology has potential benefits for trace gas detection applications, because cost, power consumption, and size of the laser pump sources can be re-

Table 2. Gas Species Detectable with Diode-Pumped DFG in PPLN[a]

Gas Species	Absorption Wavelength (μm)	Pump Wavelength (nm)	PPLN Grating Period (Calc. from Ref. 16) (μm)	Concentration Detectable with 1% Accuracy (ppb)	Air Pressure Suitable for Detection (atm)
CH_4	3.29	804	22.1	500	1
H_2CO	3.49	815	22.5	3000	0.1
HCl	3.52	817	22.6	100	1
HBr	3.78	830	22.9	500	0.1
N_2O	4.53	862	23.3	50	1
CO	4.61	865	23.3	100	1
OCS	4.87	873	23.1	50	0.1

[a]Signal wavelength of 1064.5 nm is assumed.

duced further. For example, two fiber-coupled 10–100-mW diode lasers can be used as pump sources, with one of the lasers being used in the external-cavity configuration for improved tuning range and predictability of wavelength. With bulk PPLN as the mixing element, reduction in pump power to 10-mW levels implies a factor of 750 reduction in DFG power, compromising the detection sensitivity. However, recently reported DFG conversion efficiencies for PPLN waveguide devices exceed 10% W^{-1} (Ref. 9), offering an excellent remedy for loss in pump power. Fiber coupling of the pump lasers into the waveguide would greatly improve stability of optical alignment, reduce sensitivity to vibration, reduce size, and reduce the cost of the DFG sensor.

This research was supported in part by the NASA Lyndon B. Johnson Space Center, the Texas Advanced Technology Program, the Robert A. Welch Foundation, the Department of Energy through Aerodyne Research, and the German Academic Exchange Service.

References

1. P. Canarelli, Z. Benko, R. F. Curl, and F. K. Tittel, "Continuous-wave infrared laser spectrometer based on difference frequency generation in $AgGaS_2$ for high-resolution spectroscopy," J. Opt. Soc. Am. B **9,** 197–202 (1992).
2. W. C. Eckhoff, R. S. Putnam, S. Wang, R. F. Curl, and F. K. Tittel, "A continuously tunable long-wavelength cw IR source for high-resolution spectroscopy and trace gas detection," Appl. Phys. B **63,** 437–441 (1996).
3. U. Simon, C. E. Miller, C. C. Bradley, R. G. Hulet, R. F. Curl, and F. K. Tittel, "Difference-frequency generation in $AgGaS_2$ by use of single-mode diode-laser pump sources," Opt. Lett. **18,** 1062–1064 (1993).
4. W. Schade, T. Blanke, U. Willer, and C. Rempel, "Compact tunable mid-infrared laser source by difference frequency generation of two diode-lasers," Appl. Phys. B **63,** 99–102 (1996).
5. B. Sumpf, T. Kelz, M. Nagele, and H.-D. Kronfeldt, "A cw $AgGaS_2$ difference frequency spectrometer with diode lasers as pump sources," Appl. Phys. B **64,** 521–524 (1997).
6. L. Goldberg, W. K. Burns, and R. W. McElhanon, "Difference-frequency generation of tunable mid-infrared radiation in bulk periodically poled $LiNbO_3$," Opt. Lett. **20,** 1280–1282 (1995).
7. A. Balakrishnan, S. Sanders, S. DeMars, J. Webjörn, D. W. Nam, R. J. Lang, D. G. Mehuys, R. G. Waarts, and D. F. Welch, "Broadly tunable laser-diode-based mid-infrared source with up to 31 μW of power at 4.3-μm wavelength," Opt. Lett. **21,** 952–954 (1996).
8. E. J. Lim, H. M. Hertz, M. L. Bortz, and M. M. Fejer, "Infrared radiation generated by quasi-phase-matched difference-frequency mixing in a periodically poled lithium niobate waveguide," Appl. Phys. Lett. **59,** 2207–2209 (1991).
9. M. A. Arbore, M.-H. Chou, and M. M. Fejer, "Difference frequency mixing in $LiNbO_3$ waveguides using an adiabatically tapered periodically-segmented coupling region," in *Quantum Electronics and Laser Science Conference*, Vol. 10 of 1996 OSA Technical Digest Series (Optical Society of America, Washington, D.C., 1996), p. 42.
10. Z. Feit, D. Kostyk, R. J. Woods, and P. Mak, "Molecular beam epitaxy grown PbEuSeTe buried-heterostructure lasers with continuous wave operation at 195 K," Appl. Phys. Lett. **57,** 2891–2893 (1990).
11. C. R. Webster, R. D. May, C. A. Trimble, R. G. Chave, and J. Kendall, "Aircraft (ER-2) laser infrared absorption spectrometer (ALIAS) for *in situ* stratospheric measurements of HCl, N_2O, CH_4, and HNO_3," Appl. Opt. **33,** 454–472 (1994).
12. M. Zahniser, D. D. Nelson, J. B. McManus, and P. L. Kebabian, "Measurements of trace gas fluxes using tunable diode laser spectroscopy," Philos. Trans. R. Soc. London Ser. A **351,** 371–382 (1995).
13. A. Popov, V. Sherstnev, Y. Yakovlev, R. Mücke, and P. Werle, "High power InAsSb/InAsSbP double heterostructure laser for continuous wave operation at 3.6 μm," Appl. Phys. Lett. **68,** 2790–2792 (1996).
14. Y.-H. Zhang, "Continuous wave operation of $InAs/InAs_xSb_{1-x}$ midinfrared lasers," Appl. Phys. Lett. **66,** 118–120 (1995).
15. L. E. Myers, G. D. Miller, R. C. Eckardt, M. M. Fejer, R. L. Byer, and W. R. Bosenberg, "Quasi-phase-matched 1.064-μm-pumped optical parametric oscillator in bulk periodically poled $LiNbO_3$," Opt. Lett. **20,** 52–54 (1995).
16. G. J. Edwards and M. Lawrence, "A temperature-dependent dispersion equation for congruently grown lithium niobate," Opt. Quantum Electron. **16,** 373–375 (1984).
17. W. R. Bosenberg, A. Drobshoff, J. I. Alexander, L. E. Myers, and R. L. Byer, "93% pump depletion, 3.5-W continuous-wave, singly resonant optical parametric oscillator," Opt. Lett. **21,** 1336–1338 (1996).
18. U. Simon, Z. Benko, M. W. Sigrist, R. F. Curl, and F. K. Tittel, "Design considerations of an infrared spectrometer based on different-frequency generation in $AgGaSe_2$," Appl. Opt. **32,** 6650–6655 (1993).
19. K. P. Petrov, L. Goldberg, W. K. Burns, R. F. Curl, and F. K. Tittel, "Detection of CO in air by diode-pumped 4.6-μm difference-frequency generation in quasi-phase-matched $LiNbO_3$," Opt. Lett. **21,** 86–88 (1996).
20. K. P. Petrov, S. Waltman, E. J. Dlugokencky, M. A. Arbore, M. M. Fejer, F. K. Tittel, and L. Hollberg, "Precise measurement of methane in air using diode-pumped 3.4 μm difference-frequency generation in PPLN," Appl. Phys. B **64,** 567–572 (1997).
21. L. S. Rothman, R. R. Gamache, A. Goldman, L. R. Brown, R. A. Toth, H. M. Pickett, R. L. Poynter, J.-M. Flaud, C. Camy-Peyret, A. Barbe, N. Husson, C. P. Rinsland, and M. A. H. Smith, "The HITRAN database: 1986 edition," Appl. Opt. **26,** 4058–4097 (1987).
22. A. G. Maki and J. S. Wells, *Wavenumber Calibration Tables From Heterodyne Frequency Measurements*, Spec. Publ. 821, 1991 (Natl. Inst. Stand. Technol., Gaithersburg, Md.)
23. T.-B. Chu and M. Broyer, "Intracavity CW difference frequency generation by mixing three photons and using Gaussian laser beams," J. Phys. **46,** 523–533 (1985).
24. L. E. Myers, E. L. Ginzton Laboratory, Stanford University, Stanford, Calif., 94305-4085 (personal communication, 1995).
25. W. H. Press, B. P. Flannery, S. A. Teukolsky, and W. T. Vetterling, *Numerical Recipes in Pascal* (Cambridge University, Cambridge, England, 1989), pp. 572–580.
26. F. S. Pavone and M. Inguscio, "Frequency- and wavelength-modulation spectroscopies: comparison of experimental methods using an AlGaAs diode laser," Appl. Phys. B **56,** 118–122 (1993).
27. G. Guelachvili and K. N. Rao, *Handbook of Infrared Spectroscopy* (Academic, San Diego, Calif., 1986).
28. M. Taya, M. Bashaw, and M. M. Fejer, "Photorefractive effects in periodically poled ferroelectrics," Opt. Lett. **21,** 857–859 (1996).